

Later wet seasons with more intense rainfall over Africa under future climate change

Article

Accepted Version

Dunning, C. ORCID: <https://orcid.org/0000-0002-7311-7846>,
Black, E. ORCID: <https://orcid.org/0000-0003-1344-6186> and
Allan, R. ORCID: <https://orcid.org/0000-0003-0264-9447>
(2018) Later wet seasons with more intense rainfall over Africa
under future climate change. *Journal of Climate*, 31. pp. 9719-
9738. ISSN 0894-8755 doi: 10.1175/JCLI-D-18-0102.1
Available at <https://centaur.reading.ac.uk/79325/>

It is advisable to refer to the publisher's version if you intend to cite from the work. See [Guidance on citing](#).

To link to this article DOI: <http://dx.doi.org/10.1175/JCLI-D-18-0102.1>

Publisher: American Meteorological Society

All outputs in CentAUR are protected by Intellectual Property Rights law, including copyright law. Copyright and IPR is retained by the creators or other copyright holders. Terms and conditions for use of this material are defined in the [End User Agreement](#).

www.reading.ac.uk/centaur

CentAUR

Central Archive at the University of Reading

Reading's research outputs online

1 **Later wet seasons with more intense rainfall over Africa under future**
2 **climate change**

3 Caroline M. Dunning* and Emily Black[†]

4 *Department of Meteorology, University of Reading, Reading, UK*

5 Richard P. Allan

6 *Department of Meteorology, University of Reading, Reading, UK; National Centre for Earth*
7 *Observation (NCEO)*

8 * *Corresponding author address:* Caroline M. Dunning, Department of Meteorology, University of
9 Reading, Reading, UK

10 E-mail: c.m.dunning@pgr.reading.ac.uk

11 [†]NCAS-Climate, University of Reading, Reading, UK

ABSTRACT

12 Changes in the seasonality of precipitation over Africa have high potential
13 for detrimental socio-economic impacts due to high societal dependence upon
14 seasonal rainfall. Here, for the first time we conduct a continental scale anal-
15 ysis of changes in wet season characteristics under the RCP 4.5 and RCP 8.5
16 climate projection scenarios across an ensemble of CMIP5 models using an
17 objective methodology to determine the onset and cessation of the wet season.
18 A delay in the wet season over West Africa and the Sahel of over 5-10 days on
19 average, and later onset of the wet season over Southern Africa is identified,
20 and associated with increasing strength of the Saharan Heat Low in late bo-
21 real summer, and a northward shift in the position of the tropical rain belt over
22 August-December. Over the Horn of Africa rainfall during the ‘short rains’
23 season is projected to increase by over 100mm on average by the end of the
24 21st century under an RCP 8.5 scenario. Average rainfall per rainy day is pro-
25 jected to increase, while the number of rainy days in the wet season declines in
26 regions of stable or declining rainfall (West and Southern Africa) and remains
27 constant in Central Africa, where rainfall is projected to increase. Adaptation
28 strategies should account for shorter wet seasons, increasing intensity and de-
29 creasing rainfall frequency, which will have implications for crop yields and
30 surface water supplies.

31 **1. Introduction**

32 Africa is acutely vulnerable to the effects of climate change. The large proportion of the popu-
33 lation dependent upon rain-fed agriculture for their source of income and subsistence means that
34 future changes in rainfall over Africa have high potential for detrimental socio-economic con-
35 sequences. In particular, the timing of the seasonal cycle determines the length of the growing
36 season and agricultural yields (Vizy et al. 2015), and affects the transmission period of a number
37 of vector borne diseases (Tanser et al. 2003). Understanding future changes in the seasonal cycle
38 of precipitation over Africa is crucial for establishing appropriate adaptation strategies. In order
39 to assess and interpret future projections of rainfall, we require an improved understanding of the
40 drivers and physical mechanisms behind future changes in seasonality. For the most part, coupled
41 climate models have been found to accurately represent the seasonal cycle of precipitation over
42 Africa (Dunning et al. 2017), affording the opportunity to investigate future projections and the
43 associated driving mechanisms.

44 The combination of increased atmospheric water vapour in a warming climate (Held and Soden
45 2006; Allan et al. 2010; Chou et al. 2013) with changes in atmospheric circulation, leads to a
46 complex pattern of change in rainfall over the Tropics, with changes in seasonality accompanying
47 changes in rainfall amount. Studies documenting recent enhancements in the seasonal cycle of
48 precipitation, with wet seasons getting wetter and dry seasons getting drier (Chou et al. 2013), and
49 a widening of the tropical belt (Seidel et al. 2008) altering the seasonal progression of the tropical
50 rain belt (Birner et al. 2014), imply changing rainfall seasonality in the tropics (Feng et al. 2013),
51 which will continue under future climate change (Marvel et al. 2017).

52 Previous studies have examined the changes in annual or seasonal rainfall totals over Africa
53 (Hulme et al. 2001; Lee and Wang 2014; Tierney et al. 2015; Lazenby et al. 2018). Collins et al.

54 (2013) found increases in rainfall across central equatorial Africa in boreal winter (December-
55 January-February, DJF), particularly over East Africa, with decreases over north-east Africa and
56 southern Africa for the end of the 21st Century (2081-2100). In March-April-May (MAM) Collins
57 et al. (2013) again shows increases in rainfall over central Africa and decreases over northern and
58 southern Africa. Patterns of change are similar in June-July-August (JJA) and September-October-
59 November (SON) with increases over North and North West Africa and decreasing rainfall over
60 southern Africa (Collins et al. 2013).

61 However, the societally important rainfall, that which impacts agricultural yields and affects the
62 transmission of vector borne diseases, occurs during the wet season which may not coincide with
63 fixed meteorological seasons (Cook and Vizy 2012). For example, over the Horn of Africa the
64 second wet season (short rains) occurs in October-December (Camberlin et al. 2009; Shongwe
65 et al. 2011; Yang et al. 2015a). In addition, climate model simulations may contain timing biases,
66 such as over East Africa where the first wet season (long rains; March-May) is late in coupled
67 model simulations (Dunning et al. 2017). Furthermore, other metrics are of high importance to
68 agriculturists in addition to the total amount of seasonal rainfall. The timing of the wet season,
69 and particularly the onset, determines planting dates and thus has large impacts upon agricultural
70 yields (Kniveton et al. 2009).

71 Some studies have postulated on changes in onset and cessation of the wet season by analysing
72 changes in rainfall amounts in the transition seasons or the months at the beginning and end of
73 the wet season (Biasutti and Sobel 2009; Seth et al. 2013; Sylla et al. 2015), for example, Shon-
74 gwe et al. (2009) identified a decline in austral spring (SON) rainfall over southern Africa and
75 associated this with a delay in wet season onset, and Biasutti (2013) found declining rainfall in
76 the onset months (June-July) and increasing rainfall in the demise months (September-October)
77 implying a delay in the rainy season over West Africa. However, these studies offer no quantita-

78 tive assessment of how the seasonal timing is changing and do not take into account model timing
79 biases. Furthermore, Monerie et al. (2016) found that the delay in cessation of the West African
80 monsoon was not correlated with the mean late monsoon precipitation change, although we would
81 expect changing onset and cessation dates to be related to changing rainfall at the beginning and
82 end of the wet season. Studies looking at the changing nature of seasonal timing by quantitatively
83 calculating onset and cessation dates tend to focus on the national to regional scale (Vizy et al.
84 2015) or average the results over large spatial areas, such as in Christensen et al. (2013) where
85 future projections of onset date, retreat date and duration are averaged over a North Africa and
86 Southern Africa region, masking spatial variability. Marvel et al. (2017) examined changes in the
87 seasonal cycle of zonal mean precipitation, and found a later onset at tropical latitudes; however
88 zonal averaging masks spatial variability, especially as the progression of rainfall is not always
89 zonally contiguous (Liebmann et al. 2012; Dunning et al. 2016).

90 Cook and Vizy (2012) analysed future projections of the growing season in Africa in a single
91 regional climate model, run with 6 ensemble members, with the boundary conditions determined
92 using output from 9 climate model simulations from the CMIP3 generation of models. The number
93 of growing season days is calculated by comparing precipitation to potential evapotranspiration,
94 with start and end dates computed over select regions. They find a longer growing season in the
95 central and eastern Sahel, and reductions in length of the growing season over southern Africa
96 and parts of the western Sahel. The increased resolution of the CMIP5 ensemble enables analysis,
97 previously only possible in regional models, to be carried out in global models. There is thus an
98 opportunity to advance Cook and Vizy (2012)'s results by examining changes across a number of
99 global climate models from the CMIP5 generation of models, enabling the robustness of changes
100 to be examined, using a methodology applicable across an ensemble of climate models, regardless

101 of differences in their basic state. Furthermore, we further their discussion on the mechanisms
102 behind future changes in seasonality.

103 We use an objective method for identifying the onset and cessation of the wet season, and for
104 the first time investigate changes in characteristics of African wet seasons under climate change
105 across a large ensemble of CMIP5 models at a continental scale. Decomposing the annual cycle
106 into a measure of seasonal timing and rainfall amount enables us to quantify changes in both these
107 aspects of seasonality, for regions with both one and two wet seasons per year. In addition, changes
108 in measures of rainfall intensity are also considered. This analysis is conducted across continental
109 Africa, enabling us to relate changes in seasonal timing with changes in the meteorological systems
110 that drive the seasonal cycle of rainfall over Africa.

111 **2. Methods and Data**

112 *Model output and observational data*

113 Daily precipitation data from 29 models used in the fifth phase of the Coupled Model Intercom-
114 parison Project (CMIP5, Taylor et al. 2012) was used to compute onset and cessation dates over a
115 recent period (1980-1999), a mid-21st Century period (2030-2049) and a period at the end of the
116 21st Century (2080-2099). The CMIP5 simulations include fully coupled ocean and are designed
117 to represent observed radiative forcings over the historical period while future projections use the
118 Representative Concentration Pathway (RCP) 4.5 and RCP 8.5. The RCPs comprise scenarios of
119 future changes in greenhouse gas emissions and short-lived species, and land use change, used
120 as a basis for assessing possible climate impacts (Van Vuuren et al. 2011; Thomson et al. 2011).
121 RCP 4.5 is considered an intermediate mitigation scenario, with emissions peaking around 2040,
122 and radiative forcing stabilising at 4.5 Wm^{-2} at 2100, while RCP 8.5 is a high emissions scenario,

123 with emissions rising throughout the 21st century, leading to a radiative forcing of 8.5 Wm^{-2} at
124 2100 (Van Vuuren et al. 2011; Thomson et al. 2011; Riahi et al. 2011). These two scenarios were
125 chosen to span a range of medium to high emissions future projections. Models were chosen based
126 on the availability of daily rainfall data for the required periods from the British Atmospheric Data
127 Centre (BADC). Table S1 contains a full list of models, name of institute and horizontal resolution.
128 Due to the fact that different models have different numbers of ensemble members, and the small
129 number of available ensemble members, only the first ensemble member (r1i1p1) are used.

130 Trends from the CMIP5 simulations are compared with those from the atmosphere-only simula-
131 tions from the Atmospheric Model Intercomparison Project (AMIP); daily rainfall from 28 model
132 simulations over 1979-2008 was utilised (see Table S1 in Dunning et al. (2017) for a full list of
133 models used).

134 To produce the multi-model means data were regridded using bilinear interpolation to a $1^\circ \times$
135 1° grid. For timeseries, variables were averaged over the domain used and no interpolation was
136 applied.

137 To investigate dynamical aspects of changes (Saharan Heat Low strength index and Angola Low
138 index) monthly geopotential height data (at 850 hPa and 925 hPa) was obtained for the 29 CMIP5
139 models for the historical simulation over 1980-2099 and the RCP 4.5 and RCP 8.5 simulations
140 over 2080-2099. Other variables were also obtained from BADC, including surface temperature,
141 850hPa temperature (used for calculation of potential temperature), mean pressure at sea level,
142 and relative humidity, specific humidity and u and v winds at 925hPa for the same scenarios and
143 periods.

144 Dunning et al. (2017) examined the representation of African rainfall seasonality in CMIP5
145 models, using the same method for categorising seasonal regimes and calculating onset/cessation
146 dates as is used here. The main biases identified include timing biases over the Horn of Africa

147 and an overestimation of the areal extent of the winter rainfall regime over south-west Africa.
148 Furthermore, Dunning et al. (2017) found that the coupled simulations failed to capture the biannual
149 regime over the southern West African coastline. However, for the most part Dunning et al. (2017)
150 reported that coupled climate models capture the observed patterns of seasonal progression and
151 give onset and cessation dates within 18 days of the observational dates, and thus can be used to
152 produce projections of changing seasonality.

153 In order to compare trends in AMIP and CMIP5 simulations with observed trends, a refer-
154 ence dataset was required. TAMSATv3 (Tropical Applications of Meteorology using SATellite
155 data and ground-based observations version 3) daily rainfall estimates are produced using thermal
156 infrared imagery (TIR) from Meteosat (provided by The European Organisation for the Exploita-
157 tion of Meteorological Satellites) (Schmetz et al. 2002). Rainfall estimates are calculated using
158 a time invariant calibration, based on rainfall observations from a consistent rain gauge network
159 (Tarnavsky et al. 2014; Maidment et al. 2014, 2017). The temporal consistency of both the gauge
160 measurements used and the calibration, and long time coverage (1983 onwards) makes this dataset
161 suitable for analysis of trends. Datasets which merge in rain gauge observations are not suitable,
162 as the changing rain gauge coverage can result in spurious rainfall trends (Maidment et al. 2015).
163 Rainfall data from TAMSATv3 was used for 1984-2016 and bilinearly interpolated to a $1^\circ \times 1^\circ$
164 grid. Other datasets were also considered; results produced using the Climate Hazards Group
165 InfraRed Precipitation with Stations (CHIRPS) daily precipitation dataset (Funk et al. 2015) are
166 included in the Supplementary Information for comparison. For the identification of the position
167 of the tropical rain belt daily rainfall data over land and ocean was required, thus daily precipita-
168 tion data from the Global Precipitation Climatology Project (GPCP) was used over 1997-2014 (at
169 $1^\circ \times 1^\circ$ resolution, Huffman et al. 2001).

170 *Methodology for identifying onset and cessation of rainfall seasons*

171 Onset and cessation dates were calculated using the methodology of Dunning et al. (2016) which
172 extends the methodology of Liebmann et al. (2012). For analysis of changes in onset and cessation
173 dates the method is applied separately to the three time periods used (recent period, mid 21st
174 Century and end of the 21st Century).

175 The method has three stages; full details of the method can be found in Dunning et al. (2016).
176 Firstly, the seasonal regime at each grid point is categorised as being a dominantly annual regime
177 (one wet season/ year) or biannual regime (two wet seasons/year). This is achieved by computing
178 the ratio of the amplitude of the second harmonic to the first harmonic. Next, in order to account
179 for wet seasons that span the end of the calendar year, the period of the year when the wet season
180 occurs, termed the climatological water season, is determined, by identifying the minima and max-
181 ima in the climatological cumulative daily mean rainfall anomaly. The climatological cumulative
182 daily mean rainfall anomaly is calculated by first computing the climatological mean rainfall for
183 each day of the calendar year, Q_i , and the long-term climatological daily mean rainfall, \bar{Q} . Using
184 this, the climatological cumulative daily rainfall anomaly on day d , $C(d)$, is:

$$C(d) = \sum_{i=1 \text{ Jan}}^d Q_i - \bar{Q} \quad (1)$$

185 where i ranges from 1 January to the day (d) for which the calculation applies. The minima and
186 maxima in C are used to define the beginning and end of the climatological water season. For
187 locations with a biannual regime the method extension presented in Dunning et al. (2016), not
188 included in the original method of Liebmann et al. (2012), is used to identify the climatological
189 period of the two wet seasons. Finally, onset and cessation dates are calculated for each season
190 and year individually. The daily cumulative rainfall anomaly is computed for each season; onset

191 is defined as the minima in the daily cumulative rainfall anomaly and cessation is defined as the
192 maxima. The period between the minima and maxima is a period when the rainfall is persistent
193 in occurrence, duration, and intensity (Diaconescu et al. 2015). Due to seasons spanning the end
194 of the calendar year, onset and cessation dates are not calculated for the first or last years of each
195 dataset.

196 In order to produce the timeseries over 1950-2090 the method was modified. The original
197 method does the annual/biannual categorisation over the entire period and also determines the
198 timing of the climatological water season (the period of the year when the wet season occurs)
199 over the entire period. While this is suitable for 20 year periods, it is not suitable for a 140 year
200 period, where we may expect shifts in the seasonal cycle. In order to overcome the issue of chang-
201 ing annual/biannual categorisation, maps were produced showing regions where models showed
202 a change in annual/biannual categorisation (Figure S3). The West Africa (10°W - 9°E , 7°N - 13°N)
203 and Southern Africa (20°E - 35°E , 10°S - 20°S) regions for timeseries were chosen such that almost
204 no models showed a change in regime (Figure S3). The Central Africa region was chosen to cover
205 the area that showed a large increase in wet season rainfall, with a few models showing a change
206 in regime. The multi-model-mean annual seasonal cycle over the region exhibits an annual regime
207 for both 1980-1999 (historical simulation) and 2080-2099 (RCP 8.5) and thus it was deemed that
208 an annual regime could be assumed for the entire time period over this region (Figure S3). For
209 the Horn of Africa region (land points in 35°E - 51°E , 3°S - 12°N) a biannual seasonal regime was
210 assumed and the two season method was used. If the method could not identify two wet seasons
211 per year then the point was excluded for that year.

212 The second issue, that of the timing of the climatological water season (period of the year when
213 the wet season occurs), was resolved by determining the period of the climatological water season
214 for each year individually, using a 20 year period centred on the year in question. For example,

for 1950, daily rainfall data from 1940-1959 were used to determine the beginning and end of the climatological water season. Onset and cessation dates were then calculated in the same way as described above. This adjustment should take into account any shifts in timing of the wet season.

This onset/cessation methodology identifies the period when the rainfall is persistent in occurrence, duration, and intensity, relative to the mean climate (Diaconescu et al. 2015) and has been used in a number of studies (Boyard-Micheau et al. 2013; Diaconescu et al. 2015; Monerie et al. 2016; Liebmann et al. 2017). The lack of dependence on a particular threshold facilitates the production of contemporaneous onset/cessation dates across datasets with contrasting rainfall biases (Liebmann et al. 2012; Dunning et al. 2016), enabling application to climate model simulations without the need for bias correction (Dunning et al. 2017) as the cumulative rainfall anomaly is calculated separately for each model and grid point. However, because it is a relative measure a systematic increase in rainfall will lead to no change in onset and cessation date, whereas using methods based on exceeding a rainfall threshold (e.g. Marteau et al. (2009); Issa Lélé and Lamb (2010)) would show a change in onset and cessation. Such methods, however, cannot be applied to climate model output, due to biases both in rainfall amount and occurrence, rendering methods that look for ‘no dry spell of 7 days in the next 20 days’ useless. This justified applying the cumulative rainfall anomaly method of Dunning et al. (2016), following on from Liebmann et al. (2012), which identifies changes in timing of the most persistent period of rainfall. While this method was shown to have good agreement with local indigenous methods for the present climate (Dunning et al. 2016) the same cannot be assumed for future climates. However, shifts in the timing of the periods of persistent rainfall are likely to relate to changes in timing of agricultural wet seasons, and identifying the wettest periods allows us to look at changes in physical drivers leading to these changes. The aliasing of changes in rainfall amount into changes in onset and

cessation should be taken into consideration, and seasonal cycles were checked to ensure that the changes were realistic.

Frequency and occurrence of rainfall within the wet season is also investigated. A threshold of 1mm per day was used to define a rainy day (also used in CLIMDEX indices; see <https://www.climdex.org/indices.html>); for each year and model the number of days over this threshold within the wet season (between onset and cessation) was counted, and the rainfall on these days was averaged to give the number of rainy days, and average rainfall per rainy day respectively. While some models (in particular those with higher spatial resolution, Zhang et al. 2016) may give more realistic current distributions and future changes in the frequency and occurrence of rainfall within the wet season, we have used all of the 29 CMIP5 models used in this study to produce these metrics, as present performance does not necessarily translate into more reliable future projections (Rowell et al. 2016) and extensive model evaluation would be required in order to justify the exclusion of models.

Characterisation of dynamical drivers

In order to assess changes in the seasonal progression of the Tropical Rain Belt, a method for defining the location of the InterTropical Convergence Zone (ITCZ) in terms of the peak rainfall was used (Shonk et al. 2018). Firstly, the mean daily rainfall is computed for each day of the year at each grid point. Only the region between 30°N and 30°S is considered. For each longitude and day the range of latitudes where the rainfall is greater than half of the maximum rainfall rate is considered; within this range the latitude of the rainfall centroid is taken to be the mean location of the ITCZ/ TRB. Two other definitions were also used in the analysis to establish robustness (see Supplementary Information) - the latitude of the maximum rainfall for each longitude and the latitude of the rainfall centroid (not limited to top 50%). Shonk et al. (2018) found that the

261 definition based on the rainfall centroid of the top 50% gave a smoothly varying quantity, while
262 the method based on maximum rainfall can exhibit large variations. Similar methods were also
263 used by d'Orgeval et al. (2006) and Monerie et al. (2013) to analyse changes in progression of rain
264 belts across Africa.

265 The Saharan Heat Low (SHL) and Angola Low (AL) are important drivers of rainfall seasonality
266 and variability over West Africa and the wider Sahel (Lavaysse et al. 2009) and Southern Africa
267 (Munday and Washington 2017) respectively. An index was required for quantifying the strength
268 of the SHL and AL to establish whether changes in the strength of the SHL or AL will influence
269 changing seasonality. Munday and Washington (2017) identified the AL as the lowest 5% of
270 December-January-February (DJF) mean geopotential height (at 850hPa) over southern Africa
271 (5°E - 55°E , 0° - 35°S). The strength of the AL is defined as the mean geopotential height within this
272 mask, with lower geopotential height values indicating a stronger AL. Lower level atmospheric
273 thickness is commonly used to determine the location and strength of the SHL (Lavaysse et al.
274 2009); Dixon et al. (2017a) and Dixon et al. (2017b) identified the location of the SHL to be where
275 the low-level atmospheric thickness (925-700hPa) is greater than a 90% threshold over West Africa
276 (0° - 40°N , 20°W - 30°E). The value of the 90% detection threshold quantifies the strength of the
277 SHL; a higher value indicates higher temperatures and a stronger SHL. With future climate change
278 we expect increasing lower tropospheric temperatures, resulting in higher lower level atmospheric
279 thickness (implying a stronger SHL) and higher geopotential height (implying a weaker AL).
280 Therefore, in order to compare the changing strengths of the SHL and AL, using a metric that
281 takes into account background changes in the meteorological variable used, and uses the same
282 variable to determine the strength of the SHL and AL would be more suitable.

283 An alternative methodology has been utilised by Biasutti et al. (2009) and Dixon et al. (2017a)
284 for quantifying the strength of the SHL; comparing low-level geopotential heights averaged across

the Sahara (20°N-30°N, 10°W-35°E) with the average geopotential height across the entire tropics (20°S-20°N). This comparison gives a climatological index of the local regional monsoon circulation, and in the summer months describes the strength of the SHL, while also accounting for background/large-scale changes in geopotential height. Dixon et al. (2017a) found strong correlation between this index and the index based on lower level atmospheric thickness in July-September. Here we used (15°N-30°N, 15°W-30°E) instead, to exclude the boreal summer low over Saudi Arabia, and ensure the region contained the SHL in the boreal summer months. A similar region was defined over Southern Africa, where Munday and Washington (2017) identified the AL to be; 8°S-30°S, 10°E-35°E and compared with the average geopotential height across the entire tropics (20°S-20°N) to give an index for the AL. The methods of Lavaysse et al. (2009) and Munday and Washington (2017) were used to establish the location of the SHL and AL in present and future climates; as both features are strongly constrained by topography (Chauvin et al. 2010; Evan et al. 2015; Munday and Washington 2017; Howard and Washington 2018) no large shifts in location are expected and thus such metrics can be utilised (see Supplementary Information).

Biasutti et al. (2009) and Dixon et al. (2017a) used geopotential height at 925 hPa for the SHL while Munday and Washington (2017) used 850 hPa for the AL due to lower levels intersecting with topography in some CMIP5 models. Here geopotential height at 925 hPa was used for the SHL and 850hPa geopotential height was used for the AL. The Supplementary Information includes results for both 850hPa and 925hPa geopotential height for both regions and consistent results were obtained (Figure S16-17). Dixon et al. (2017a) noted that this metric describes the strength of the regional monsoon circulation, and only describes the strength of the low during the summer months, when the low is within the regions defined; when discussing results the distinction between the strength of the regional monsoon circulation and strength of the SHL/AL will be noted.

3. Changing Rainfall Seasonality and Characteristics

Figure 1 shows the median change in onset, cessation, wet season length and seasonal rainfall from 1980-1999 to 2080-2099 (RCP 8.5 scenario) across 29 CMIP5 models. For the RCP 4.5 scenario, a mid-range scenario with a smaller climate change signal than RCP 8.5, consistent spatial patterns of change were found, although generally of smaller magnitude (see Supplementary Information). Spatial patterns were also consistent for the mid-century period, though changes were very small (results not shown). Wet season onset is projected to get later across much of West Africa and the southern Sahel, and over a north-west/south-east orientated strip across southern Africa, with the largest changes of over 12 days on average over parts of Angola, Zimbabwe and Mozambique (8 days for RCP 4.5). West of 0°W, and at all longitudes between 10°N and 20°S, more than 75% of the CMIP models used agree that the onset will get later. In the regions with an annual regime 0°-20°N, Figure 1b shows cessation of the wet season getting later, which combined with Figure 1a, indicates the wet season over West Africa and the Sahel is shifting later in the calendar year, with little change in length, confirmed in Figure 1c. Across West Africa and the Sahel, there is good model agreement (>75% of models) that cessation will get later. This is consistent with the increase in late wet season rainfall found in other studies (Biasutti and Sobel 2009; Biasutti 2013; Seth et al. 2013; Monerie et al. 2016). Sylla et al. (2015) found the largest reduction in rainfall in the pre-monsoon and mature monsoon phase west of 5°W and Monerie et al. (2017) also found a decrease in precipitation over the western Sahel; this is in agreement with the largest delay in onset west of 0-5°W presented in Figure 1a. Cook and Vizzy (2012) found a reduction in the number of growing season days west of 0°W associated with a delay in onset, where Figure 1 also shows onset getting later and a reduction in season length, however Cook and Vizzy (2012) also found increases in spring rainfall to the east of this, with an earlier onset, not found

332 in this study or others (Biasutti and Sobel 2009; Lee and Wang 2014; Seth et al. 2013; Sylla et al.
333 2015). Across West Africa and the Sahel they find delays in the end date of 8-10 days on average,
334 in agreement with the results in Figure 1. Dunning et al. (2017) found that the coupled CMIP5
335 models did not capture the correct seasonal regime over the southern West African coastline, thus
336 results there should be viewed with caution.

337 Over Southern Africa, the later onset results in a shorter wet season, with a reduction in total wet
338 season rainfall centred on the Angola/ Namibia/ Botswana/ Zambia border, with more than 75% of
339 the models agreeing on a reduction in rainfall. Similarly, Cook and Vizzy (2012) found a reduction
340 in growing season days across Angola and southern Democratic Republic of the Congo associated
341 with a decline in austral spring rainfall leading to a later onset. Figure 1b shows earlier cessation
342 over Namibia and Botswana, but very few models indicate a statistically significant change here.
343 Shongwe et al. (2009) also identified a decline in austral spring rainfall over Mozambique and
344 Zimbabwe, which they associated with a delay in the onset. To the north of the equator, in central
345 regions, wet season rainfall is projected to increase, with strong model consensus and the largest
346 statistically significant changes found over Cameroon, southern Chad and the surrounding regions,
347 with average increases greater than 75mm over 15°E-30°E, 5°N-11°N (50mm for RCP 4.5), also
348 found by Cook and Vizzy (2012). Little change in total wet season rainfall is found west of 5°E.
349 Over northern Tanzania there is little change in seasonal timing, but an increase in total wet season
350 rainfall.

351 The central equatorial region and Horn of Africa experience two wet seasons per year; projec-
352 tions for the ‘long rains’ (boreal spring wet season) and ‘short rains’ (boreal autumn wet season)
353 are shown in Figure 2. Earlier cessation of the long rains and later onset of the short rains implies
354 a longer boreal summer dry season; however these changes are less than a week on average and
355 only statistically significant over small areas. The most notable changes are for the short rains;

Figure 2d,h shows the end of the short rains occurring over 8 days later on average (similar value for RCP 4.5), and substantial increases in rainfall amount, similar to the findings in Shongwe et al. (2011) and Cook and Vizzy (2012). There is strong model consensus, with more than 75% of the models agreeing on later cessation and heavier rainfall across the region. Coupled climate simulations for the historical period overestimate the short rains and underestimate the long rains relative to observations; thus projections of increasing short rains should be viewed with caution (Tierney et al. 2015; Yang et al. 2015b; Dunning et al. 2017). The pattern of surface warming in the Indian Ocean shows greater warming in the northwest Indian Ocean compared to the south east Indian Ocean (Zheng et al. 2013), implying an increasingly positive Indian Ocean Dipole (IOD) (results not shown). Positive IOD leads to increased rainfall over East Africa, particularly during the short rains (Black et al. 2003; Shongwe et al. 2011), which may contribute to the longer and wetter short rains in Figure 2. Further south, Funk et al. (2008) found that warming of the Indian Ocean disrupted onshore moisture transports leading to reduced growing season rainfall over South-East Africa. Shongwe et al. (2009) also found a substantial weakening of moisture transport from the Indian Ocean along the south-east coast of southern Africa, related to reduced austral spring rainfall and a later onset. Thus, the pattern of warming in the Indian Ocean may enhance the short rains over the Horn of Africa (Figure 2), and lead to later onset and reduced rainfall over Southern Africa (Figure 1). However, Lazenby et al. (2018) did not find sufficient evidence of a link between changing OND rainfall over Southern Africa and changing SST gradients.

In addition to the onset and cessation, the manner in which precipitation occurs also impacts agriculturalists and other stakeholders. Long, dry periods can reduce soil moisture and harden the surface layer, thus when heavy rainfall events do occur a smaller fraction infiltrates into the root layer and increased runoff leads to soil erosion (Black et al. 2016). Additionally, heavy rainfall can adversely affect crops such as coffee and cocoa, where intense rainfall may lead to the damage of

380 the flowers (Rosenthal 2011; Frank et al. 2011; Hutchins et al. 2015). Figure 3 shows the change in
 381 average rainfall per rainy day and number of rainy days in the wet season (where a rainy day is any
 382 day with rainfall ≥ 1 mm during the wet season), in addition to changes in onset and total wet season
 383 rainfall over part of Southern Africa (20°E-35°E, 10°S-20°S). While there is only a small change
 384 in total seasonal rainfall (Figure 3b), there is a significant decrease in the number of rainy days
 385 (10 fewer per wet season on average in 2090 compared to 1980-2000), and increase in the average
 386 rainfall per rainy day (increase of >0.75 mm/day on average in 2090 compared to 1980-2000;
 387 Figure 3c-d). Similarly, Sillmann et al. (2013) found a decline in the number of heavy precipitation
 388 days, more consecutive dry days and a higher percentage of rainfall coming from very wet days
 389 over this region. The observations exhibit much interannual variability, with none of the trends
 390 statistically significant at the 5% level (Wald Test, with the null hypothesis that the slope is zero).
 391 Over 1985-2007, timeseries from TAMSATv3 and the coupled simulations all show increasing
 392 rainfall per rainy day (TAMSATv3 - 0.30 mm/day/decade), in agreement with future trends. While
 393 overall there is a slight increase in the number of rainy days, there are large interannual variations.
 394 Precipitation estimates based on infrared radiation, such as TAMSATv3, do not capture daily
 395 extremes well, so may not simulate this aspect of climate change accurately (Maidment et al. 2014,
 396 2017). Similar patterns of increasing intensity under future climate change are found over West
 397 Africa (20°E-35°E, 10°S-20°S, Figure S4), with increasing rainfall per rainy day over 1985-2007
 398 in TAMSATv3, AMIP and the coupled simulations, with trends ranging from 0.09mm/day/decade
 399 to 0.12mm/day/decade, and future projections of decreasing numbers of rainy days, with decreases
 400 of 5-10 rainy days on average in 2090 compared to 1980-2000. Taylor et al. (2017) identified an
 401 increase in the frequency of intense storms over the Sahel since 1982, associated with Saharan
 402 warming and an increased meridional temperature gradient. Increasing rainfall per rainy day may
 403 explain the non-statistically significant change in rainfall over Mauritania and Senegal (Figure 1d),

404 despite the statistically significant reduction in season length (Figure 1c), associated with the later
405 onset (Figure 1a). Central Africa (15°E-30°E, 5°N-11°N) exhibits increasing average rainfall per
406 day, both over the observational and future period, and little long term change in number of rainy
407 days (Figure S5), consistent with the increase in seasonal rainfall shown in Figure 1d. Other
408 studies have identified similar trends over Southern Africa (Sylla et al. 2015; Pohl et al. 2017) and
409 at wider scales (Cubasch et al. 2001); here we have identified that the same changes occur within
410 the wet season, with the change in number of rainy days potentially important for determining
411 changes in overall seasonal rainfall.

412 Figure 4 shows the observed and projected changes in cessation of the wet season over West
413 Africa (10°W-9°E, 7°N-13°N) and Central Africa (15°E-30°E, 5°N-11°N), and cessation of the
414 ‘short’ rains (boreal autumn wet season over the Horn of Africa; land points in 35°E-51°E, 3°S-
415 12°N). Dunning et al. (2016) showed that the cessation of the short rains follows on from the
416 cessation of the main wet season over West Africa and the Sahel, associated with the southward
417 retreat of the rain belt in boreal autumn. The projections indicate cessation shifting later in all
418 three regions in the future with multi-model mean changes of up to 10 days (Figure 4). Observed
419 trends from TAMSATv3 and AMIP simulations also show cessation getting later, with particularly
420 strong trends in TAMSATv3 over the Central Africa region, with trends of around 5 days/decade
421 over 1985-2007 (Figure 4b). Agreement between future projections, AMIP and observed trends
422 adds credence to future projections.

423 Timeseries for the West African region shows the best AMIP/TAMSATv3 agreement compared
424 to the other regions with trends of 1.8 days/decade and 2.5 days/decade over 1985-2007 respec-
425 tively. Some of this trend is likely to be attributable to the recent rainfall recovery over Sahel
426 region, following the devastating drought in the 1980s (Biasutti et al. 2009; Nicholson 2013; Evan
427 et al. 2015), but it is also strongly influenced by decadal climate variability (Maidment et al.

2015). Figure 4c shows cessation of the short rains getting later by 4.2 days/decade over 1985-2007 (TAMSATv3), with much interannual variability. Agreement of future projections with past trends may add additional confidence to future projections, though the trends in TAMSATv3 and AMIP are larger than those from the coupled simulations in all three regions, they are more likely to reflect internal climate variability not represented by ensemble mean simulations.

In summary, CMIP5 projections show changes in the seasonal timing of the wet season over Africa. A delay in the wet season is projected over West Africa and the Sahel, with recent trends showing the cessation of the wet season getting later. Over Southern Africa a later onset results in a shorter wet season, and reduced total wet season rainfall. Increasing rainfall is projected for the ‘short rains’ over the Horn of Africa, with a later end to the season. Model agreement, with >75% of the models agreeing on the sign of the change indicates robustness, and agreement with observations and AMIP adds credence. Within the wet season average rainfall per rainy day is projected to increase, while the number of rainy days is projected to decline in regions of stable or declining rainfall and remain constant in Central Africa, where rainfall is projected to increase. In the next section possible drivers of such changes will be explored.

4. Links between the Saharan Heat Low, the Angola Low and Later Onset/Cessation of Wet Seasons

The seasonal progression of rainfall over Africa is driven by complex interaction of a number of factors (Nicholson 2000; Sultan and Janicot 2003; Lavaysse et al. 2009; Nicholson 2013; Lazenby et al. 2016; Munday and Washington 2017; Nicholson 2017). In this section links between the seasonal progression of the tropical rain belt, and the strength of the Angola Low and Saharan Heat Low are explored.

450 The northward and southward progression of the tropical rain belt, following the maximum in-
451 coming solar radiation is one of the major drivers of the seasonal cycle of precipitation across
452 Africa. The Saharan Heat Low and Angola Low form over northern and southern Africa re-
453 spectively during the local summer, and cyclonic circulation associated with these features leads
454 to significant transport of moisture onto the continent from the neighbouring oceans (Nicholson
455 2013; Lazenby et al. 2016). Comparing responses across the ensemble of CMIP5 models, and in-
456 specting outliers, enables us to utilize the CMIP5 ensemble as a ‘testbed’ to examine mechanistic
457 hypotheses.

458 The trend of cessation getting later over West Africa and the Sahel, onset getting later over
459 Southern Africa, combined with the later shift of the short rains, suggests a change in the progres-
460 sion of the tropical rain belt during the second half of the calendar year. Separate studies have
461 identified factors suggesting both the later shift of cessation over the Sahel (Biasutti and Sobel
462 2009; Seth et al. 2013; Monerie et al. 2016) and later onset over South East Africa (Shongwe et al.
463 2009). Biasutti and Sobel (2009) associated a delay in the seasonal cycle of precipitation with
464 changes in the SST seasonal cycle. Seth et al. (2013) found a redistribution of monsoon rainfall
465 from early to late in the monsoon season, with a reduction in early season rainfall the consequence
466 of an enhanced convective barrier resulting from reduced moisture availability. Dwyer et al. (2014)
467 found a global amplification and phase delay of the seasonal cycle of precipitation, with the de-
468 lay attributed to changes in the seasonality of the circulation. In this section we investigate factors
469 affecting the delay in the cessation over West Africa and the Sahel, and onset over Southern Africa.

470 *a. Background on the Saharan Heat Low and Angola Low*

471 During the boreal summer high insolation and low evaporation over the Sahara leads to the
472 formation of an intense heat low (Lavaysse et al. 2009; Dixon et al. 2017a), termed the ‘Saharan

473 Heat Low' (SHL), with high surface temperatures and low surface pressures (Lavaysse et al. 2009;
474 Parker and Diop-Kane 2017). The associated cyclonic circulation increases the north easterly
475 Harmattan flow and south westerly monsoon flow (Lavaysse et al. 2009; Nicholson 2013; Parker
476 and Diop-Kane 2017), that transports moisture rich air into the Sahel region, fuelling convection
477 and precipitation (Dixon et al. 2017b) and thus forms a key part of the West African Monsoon
478 (Chauvin et al. 2010; Nicholson 2013). Variations in both the strength and position of the SHL
479 have been shown to affect the onset of the monsoon and total seasonal rainfall (Lavaysse et al.
480 2009; Biasutti and Sobel 2009; Chauvin et al. 2010; Park et al. 2016; Dixon et al. 2017a), as
481 well as intraseasonal variations, including monsoon 'bursts' (Nicholson 2013; Parker and Diop-
482 Kane 2017). Furthermore, Chauvin et al. (2010) found intraseasonal variability of the SHL was
483 associated with midlatitude intraseasonal variability.

484 Future projections indicate strengthening and deepening of the SHL leading to increasing Sahel
485 rainfall (Biasutti and Sobel 2009; Monerie et al. 2016; Vizy and Cook 2017). Enhanced tempera-
486 tures over the Sahara act to deepen the SHL and enhance monsoon flow, bringing more moisture
487 into the region. Water vapour is a greenhouse gas, leading to further temperature increases (Evan
488 et al. 2015; Vizy and Cook 2017). Variations in dust aerosol have also been linked with variations
489 in the strength of the SHL (Alamirew et al. 2018) and Sahel precipitation (Konare et al. 2008;
490 Solomon et al. 2008).

491 The Angola Low (AL) forms over a plateau region in southern Angola/northern Namibia in aus-
492 tral summer, at the southern limit of a trough of low pressure extending from Ethiopia, through
493 Central Africa, associated with the intertropical convergence zone (Reason et al. 2006; Munday
494 and Washington 2017). Variations in the strength of the AL have been associated with both daily
495 (Crétat et al. 2018) and interannual precipitation variability (Cook et al. 2004; Munday and Wash-
496 ington 2017) over Southern Africa. Howard and Washington (2018) found that on a synoptic

scale the AL can be separated into the Angola Heat Low and Angola Tropical Low, with the precipitation variability more strongly related to the interannual variability of the tropical lows. Increased westerlies from the south-east Atlantic, associated with strengthened AL circulation, increase low-level moisture in this region, increasing the formation of tropical-extratropical cloud bands and precipitation (Cook et al. 2004; Reason et al. 2006; Lazenby et al. 2016; Munday and Washington 2017). Conversely, Cook et al. (2004) found that dry late summers (January-March) were associated with a decrease in the strength of the AL.

b. Future changes in SHL and AL

Given the important role that the SHL and AL play in driving rainfall seasonality and variability over West Africa and the wider Sahel (Lavaysse et al. 2009) and Southern Africa (Munday and Washington 2017; Crétat et al. 2018; Howard and Washington 2018), their influence in a changing climate was investigated. A metric based on the methodology of Biasutti et al. (2009) and Dixon et al. (2017a) was used to quantify changes in the strength of the SHL and AL (see section 2). This index describes the strength of the regional circulation throughout the year; during the boreal/austral summer it describes the strength of the SHL/AL respectively (Dixon et al. 2017a). The location of the two regions used to define the strength of the SHL and AL is shown in Figure 5, with the colours showing the multi-model mean increase in 850 hPa potential temperature over JJA (a) and DJF (b). The largest increases in temperature are found across North Africa, north of 20°N in JJA. Over the AL region a smaller increase in potential temperature is found in both JJA and DJF.

Comparison of the relative strength of the SHL and AL in the historical and future simulations shows an increase in the strength of the SHL/northern regional circulation in June-September, with the largest increases toward the end of the boreal summer (Figure 6c,e) as found in Biasutti et al.

(2009). Recent increasing greenhouse gas concentrations have been shown to act to strengthen the West African Monsoon circulation and the SHL (Dong and Sutton 2015), and storm intensity (Taylor et al. 2017), with continuing emissions likely to contribute to future strengthening. The magnitude of the increase in strength of the AL in austral summer is similar to the increase in strength of the southern regional circulation throughout the entire year, and is of lower magnitude than the increase in strength of the SHL in the late boreal summer months (Figure 6c-e). This is consistent with the increases in potential temperature seen in Figure 5.

c. Change in the progression of the Tropical Rain Belt

The method of Shonk et al. (2018) was used to identify the mean position of the tropical rain belt (TRB) in CMIP5 simulations (see section 2) to assess whether a change in seasonal progression of the TRB was observed. Figure 6a-b shows the mean seasonal progression of the TRB and its response to climate change over 0°E-35°E. The analysis was repeated using two other definitions for TRB (latitude of maximum rainfall and latitude of rainfall centroid with rainfall not limited to top 50%; see section 2); similar results were obtained, suggesting that the analysis is robust to TRB definition (see Supplementary Information). Figure 6a demonstrates agreement between the seasonal progression of the TRB in observations and CMIP5 models; the main difference is between January and March/April. Under RCP 8.5 the southward progression of the TRB shifts later in the year; the TRB is on average 0.8-1.2° north of its position in the historical simulation from August to December. When viewed from a single latitude the passage of the TRB occurs up to 15 days later. This is consistent with the trends seen in onset and cessation (Figure 1- 2); a later southward progression leads to a later cessation over West Africa and later onset over Southern Africa. Using similar methods, d'Orgeval et al. (2006) also found a northward shift in the location of the rain belt in October and Monerie et al. (2013) identified a northward shift

543 from August-November, when considering the region from 0°E-25°E, 10°S-21°N. Analysis with
544 an observational dataset (GPCP 1DD, as daily rainfall data over land and ocean was required,
545 Huffman et al. 2001) confirms that later southward progression of the TRB is associated with
546 later cessation and onset over West Africa and the Sahel, and Southern Africa respectively (see
547 Supplementary Information and Figure S11). Maidment et al. (2014) showed high correlation
548 between GPCP and TAMSAT rainfall, and Dunning et al. (2016) shows good agreement between
549 onset/cessation dates produced using TAMSAT and GPCP 1DD.

550 The later onset over West Africa is mostly significant west of 0°W (Figure 1). The change in
551 position of the TRB was analysed separately over this region. Between 0°W - 16°W a southward
552 shift in the mean position of the TRB is apparent from January-June under the RCP scenarios
553 compared with historical (1980-1999, see Supplementary Information). This is consistent with
554 the later onset in Figure 1a. Other studies have linked reduced early season precipitation over
555 West Africa with lower relative humidity resulting from reduced moisture convergence (Seth et al.
556 2013) related to south-westerly flow anomalies carrying more moisture to the east (Cook and Vizzy
557 2012, see Supplementary Information).

558 *d. Links between the Saharan Heat Low, the Angola Low and progression of the Tropical Rain* 559 *Belt*

560 We postulate that the increase in strength of the SHL, associated with higher surface temper-
561 atures, lower surface pressure and lower geopotential height over the region, toward the end of
562 the boreal summer, is causing the TRB to move further north in July and August (Figure 6a-b).
563 This in turn delays the southward progression, thus giving a later cessation of the wet season over
564 West Africa and the Sahel, and is one of the factors contributing to the later short rains over the
565 Horn of Africa, and later onset of the main wet season over Southern Africa. The changes associ-

ated with the strengthening of the SHL/northern regional circulation (higher surface temperatures, lower surface pressure (Figure 7, Figure S18) and lower geopotential height), toward the end of the boreal summer, favour moisture convergence over the northern part of Africa. Figure 7 shows greater transport of moisture into the Sahel region, both southerly from the Gulf of Guinea and northerly from the Mediterranean (partly linked to increased moisture over the Mediterranean), and northward anomalies around the equator. Monerie et al. (2016) also found a northward shift of the monsoon, and increased moisture transport from the Mediterranean Sea. This is likely to be linked to later cessation over this region found in Figure 1b. Additionally, there is less moisture transport into southern Africa, with reduced relative humidity in August-October (Figure 7, Figure S18). Seth et al. (2013) associated later onset over Southern Africa with reduced boundary layer moisture availability at the end of the dry season, resulting from reduced moisture convergence and lower evaporation. Thus, changes in moisture transport associated with changes in the strength of the SHL may influence relative humidity over Southern Africa and delay the start of the wet season, although other drivers, including changes in pressure and surface temperatures over the neighbouring oceans are also likely to play a role (Funk et al. 2008; Shongwe et al. 2009; Lazenby et al. 2018).

In order to test the hypothesis that the increase in strength of the SHL and regional circulation over North Africa toward the end of the boreal summer delays the southward progression of the TRB, the increase in strength of the SHL in 29 CMIP5 models is plotted against the mean change in TRB position (Figure 6f). Models with a larger increase in strength of the SHL in July-August also exhibited a larger northward shift in the position of the TRB in August - December, and conversely, models with a smaller amplification of the SHL such as EC-Earth have a smaller change in TRB position (Figure 6f) with the correlation coefficient statistically significant at the 5% confidence level. In their analysis of one regional climate model, Cook and Vizy (2012) related

590 a deepening of the SHL with increased south westerly monsoon flow and a delay in the wet season
591 over the Sahel; we have extended this by testing the hypothesis quantitatively across the CMIP5
592 ensemble. Further analysis, with targeted model simulations and analysis is required to confirm
593 this connection.

594 The limited increase in strength of the SHL under RCP 8.5 in EC-Earth is potentially related
595 to less warming over North Africa (10°W-60°E, 20°N - 50°N) in July-September and over the
596 Mediterranean during July-August (lowest 10% of the 29 CMIP5 models used in this analysis).
597 Furthermore, EC-Earth also doesn't capture the boreal summer amplified warming over North
598 Africa, Southern Europe, the Mediterranean Sea and central Asia compared with the global tem-
599 perature increase, seen in other CMIP5 models, indicating some of the difference may be related to
600 the simulated amplification of land sea temperature contrast (Sutton et al. 2007; Joshi et al. 2008;
601 Lambert et al. 2011).

602 In summary a northward shift in the mean position of the tropical rain belt in August-December
603 (and consequent later southward progression of the tropical rain belt) and later onset/cessation of
604 the wet season has been identified and linked with increasing strength of the Saharan Heat Low.
605 Simulations with stronger amplification of the heat low experience a greater delay in the southward
606 progression of the Tropical Rain Belt.

607 **5. Conclusions**

608 In conclusion, an objective methodology has been used to investigate changes in the characteris-
609 tics of African wet seasons under climate change across 29 CMIP5 models. Additionally, changes
610 in large scale drivers of the seasonal cycle of precipitation over Africa are investigated to explore
611 the physical mechanisms underlying future changes.

612 Our key findings are:

- A pattern of increasing rainfall intensity was identified, with higher average rainfall per rainy day found across regions of West Africa, Southern Africa and Central Africa. Combined with a decline in the number of rainy days this leads to little change, or a slight decline in the total wet season rainfall over West and Southern Africa. Over Central Africa the combination of increasing rainfall per rainy day with little change in the number of rainy days leads to increases in the total seasonal rainfall.
- Large parts of Southern Africa are projected to experience a later onset date, with changes of around 12 days over Angola, as well as a shorter wet season and less wet season rainfall.
- Over the Horn of Africa, which experiences two wet seasons per year, the second wet season ('short rains') is projected to end over a week later, with a large increase in seasonal rainfall.
- Over West Africa/ the Sahel both onset and cessation are projected to get later, with the entire wet season shifting 5-10 days later in the calendar year, and little overall change in the length of the wet season.
- The southward retreat of the tropical rain belt is projected to shift later in the calendar year, consistent with the trends of later cessation over West Africa and the Sahel, later short rains and later onset over Southern Africa. On average the tropical rain belt is projected to be 0.8-1.2° north of its previous position over August-December.

Large increases in surface temperature over the Sahara and North Africa during the boreal summer months lead to an intensification of the Saharan Heat Low. Smaller changes are identified in the strength of the Angola Low. Thus it is proposed that the higher temperatures and lower surface pressure and geopotential height means that the tropical rain belt travels further north and stays north longer, delaying the southward retreat, although other factors (including changing SST) are also likely to alter rainfall seasonality further south. Across the 29 CMIP5 models used we found

636 strong correlation between the increase in strength of the SHL and the shift in the TRB position,
637 with models that had a larger increase in the strength of the SHL exhibiting a larger shift in the
638 position of the TRB. A number of other factors may also play a role, but the analysis of these
639 factors is beyond the scope of this study.

640 Previously, Cook and Vizzy (2012) analysed future projections of the growing season across
641 Africa in a single regional climate model, and proposed that delay in the wet season over the Sahel
642 was related to the deepening of the SHL. We found consistent results when we tested the SHL/
643 wet season delay hypothesis quantitatively across the CMIP5 ensemble.

644 Further analysis is required to explore inter-model differences, and the impacts of other drivers.
645 For example, a number of studies have identified the role of warming in the Western Indian Ocean
646 on moisture transport over Southern Africa (Funk et al. 2008; Shongwe et al. 2009), although
647 Lazenby et al. (2018) found no robust link between austral spring rainfall and changing SST gra-
648 dients. They commented on the potential role of South Atlantic high pressure as a driver of chang-
649 ing onset (Reason et al. 2006), but did not investigate this further. Seth et al. (2013) associated
650 spring precipitation decreases across Southern Africa with declining moisture convergence and
651 reduced evaporation. In this study, we found no robust link between an increase in the strength of
652 the Angola Low and changing seasonality. Thus, investigating the role of other drivers, including
653 pressure patterns over the South Atlantic and different patterns of Indian Ocean warming on the
654 seasonal cycle of precipitation would be interesting extension. Fully understanding inter-model
655 differences in projected changes in the Saharan Heat Low would also advance this work further.

656 Dunning et al. (2017) identified some discrepancies in the representation of the seasonal cycle
657 in coupled CMIP5 simulations; namely timing biases over the Horn of Africa and an overestimate
658 of the short rains, an overestimate of the region experiencing a winter rainfall regime over south-
659 west Africa and an incorrect seasonal cycle over the southern West African coastline. Thus future

660 projections for these regions should be viewed with caution. Model improvements, that reduce
661 such biases in coupled simulations are needed to produce reliable future projections over such
662 regions.

663 In conclusion, future climate change will lead to a shift in the timing of wet seasons over Africa,
664 with a delay in the wet season over West Africa and the Sahel, and later onset leading to a reduc-
665 tion in season length over Southern Africa. This may have implications for crop development, as
666 a shorter growing season may mean that crops do not reach full maturity. Additionally, increasing
667 intensity of rainfall may adversely affect crops, particularly at certain times during coffee devel-
668 opment. Further work is required to investigate additional drivers, and their interactions, as well
669 as attribution of inter-model differences.

670 *Acknowledgments.* The authors would like to thank two anonymous reviewers for their helpful
671 comments.

672 We acknowledge the World Climate Research Programme’s Working Group on Coupled Mod-
673 elling, which is responsible for CMIP, and we thank the climate modeling groups (models listed in
674 Table S1) for producing and making available their model outputs; for CMIP, the U.S. Department
675 of Energy’s PCMDI provided coordinating support and led development of software infrastructure
676 in partnership with the Global Organization for Earth System Science Portals. Model data were
677 sourced from the CMIP5 data portal (http://cmip-pcmdi.llnl.gov/cmip5/data_portal.html) and the
678 British Atmospheric Data Centre (<http://badc.nerc.ac.uk/>).

679 All observational datasets exploited are publicly available datasets. The TAMSATv3 dataset is
680 available from the TAMSAT website (<http://www.met.reading.ac.uk/~tamsat/data>). GPCP daily
681 data are available from <http://precip.gsfc.nasa.gov/>. The CHIRPS dataset, produced by the Climate
682 Hazards Group, is available at http://chg.geog.ucsb.edu/data/chirps/#_Data.

683 Caroline M. Dunning is supported with funding from a Natural Environment Research Coun-
 684 cil (NERC) PhD Studentship through the SCENARIO Doctoral Training Partnership grant
 685 NE/L002566/1. Richard P. Allan’s contribution to the research leading to these results has re-
 686 ceived funding from the National Centre for Earth Observation and the European Union 7th
 687 Framework Programme (FP7/2007-2013) under grant agreement 603502 (EU project DACCIWA:
 688 Dynamics-aerosol-chemistry-cloud interactions in West Africa). Emily Black’s contribution to the
 689 research has been supported by the National Centre for Atmospheric Science (Climate division)
 690 ACREW project, which is supported by NERC and the Global Challenges Research Fund. She
 691 also gratefully acknowledges support from the NERC/DFID BRAVE project (NE/M008983/1),
 692 the NERC/DFID HyCristal project (NE/M020371/1) and the Global Challenges Research Fund
 693 project, SatWIN-ALERT (NE/R014116/1). We are grateful to the Mars Wrigley Confectionery
 694 research team for stimulating discussions on the wider context and applications of this work.

695 **References**

- 696 Alamirew, N. K., M. C. Todd, C. L. Ryder, J. H. Marsham, and Y. Wang, 2018: The early sum-
 697 mertime Saharan heat low: sensitivity of the radiation budget and atmospheric heating to water
 698 vapour and dust aerosol. *Atmospheric Chemistry and Physics*, **18** (2), 1241–1262.
- 699 Allan, R. P., B. J. Soden, V. O. John, W. Ingram, and P. Good, 2010: Current changes in tropical
 700 precipitation. *Environmental Research Letters*, **5** (2), 025 205.
- 701 Biasutti, M., 2013: Forced Sahel rainfall trends in the CMIP5 archive. *Journal of Geophysical*
 702 *Research: Atmospheres*, **118** (4), 1613–1623.
- 703 Biasutti, M., and A. H. Sobel, 2009: Delayed Sahel rainfall and global seasonal cycle in a warmer
 704 climate. *Geophysical Research Letters*, **36** (23).

705 Biasutti, M., A. H. Sobel, and S. J. Camargo, 2009: The role of the Sahara low in summertime
706 Sahel rainfall variability and change in the CMIP3 models. *Journal of Climate*, **22** (21), 5755–
707 5771.

708 Birner, T., S. M. Davis, and D. J. Seidel, 2014: The changing width of earth s tropical belt. *Physics*
709 *Today*, **67** (12).

710 Black, E., H. Greatrex, M. Young, and R. Maidment, 2016: Incorporating Satellite Data Into
711 Weather Index Insurance. *Bulletin of the American Meteorological Society*, **97** (10), ES203–
712 ES206.

713 Black, E., J. Slingo, and K. R. Sperber, 2003: An observational study of the relationship between
714 excessively strong short rains in coastal East Africa and Indian Ocean SST. *Monthly Weather*
715 *Review*, **131** (1), 74–94.

716 Boyard-Micheau, J., P. Camberlin, N. Philippon, and V. Moron, 2013: Regional-scale rainy season
717 onset detection: a new approach based on multivariate analysis. *Journal of Climate*, **26** (22),
718 8916–8928.

719 Camberlin, P., V. Moron, R. Okoola, N. Philippon, and W. Gitau, 2009: Components of rainy
720 seasons variability in Equatorial East Africa: onset, cessation, rainfall frequency and intensity.
721 *Theoretical and Applied Climatology*, **98** (3-4), 237–249.

722 Chauvin, F., R. Roehrig, and J.-P. Lafore, 2010: Intraseasonal variability of the Saharan heat low
723 and its link with midlatitudes. *Journal of Climate*, **23** (10), 2544–2561.

724 Chou, C., J. C. Chiang, C.-W. Lan, C.-H. Chung, Y.-C. Liao, and C.-J. Lee, 2013: Increase in the
725 range between wet and dry season precipitation. *Nature Geoscience*, **6** (4), 263–267.

Christensen, J. H., K. K. Kanikicharla, G. Marshall, and J. Turner, 2013: Climate phenomena and their relevance for future regional climate change. *In: Climate Change 2013: The Physical Science Basis. Contribution of Working Group I to the Fifth Assessment Report of the Intergovernmental Panel on Climate Change.*

Collins, M., and Coauthors, 2013: Long-term climate change: projections, commitments and irreversibility. *In: Climate Change 2013: The Physical Science Basis. Contribution of Working Group I to the Fifth Assessment Report of the Intergovernmental Panel on Climate Change.*

Cook, C., C. J. Reason, and B. C. Hewitson, 2004: Wet and dry spells within particularly wet and dry summers in the South African summer rainfall region. *Climate Research*, **26** (1), 17–31.

Cook, K. H., and E. K. Vizy, 2012: Impact of climate change on mid-twenty-first century growing seasons in Africa. *Climate Dynamics*, **39** (12), 2937–2955.

Crétat, J., B. Pohl, B. Dieppois, S. Berthou, and J. Pergaud, 2018: The Angola Low: relationship with southern African rainfall and ENSO. *Climate Dynamics*, doi:10.1007/s00382-018-4222-3.

Cubasch, U., and Coauthors, 2001: Projections of future climate change. 526–582 pp.

Diaconescu, E. P., P. Gachon, J. Scinocca, and R. Laprise, 2015: Evaluation of daily precipitation statistics and monsoon onset/retreat over western Sahel in multiple data sets. *Climate Dynamics*, **45** (5-6), 1325–1354.

Dixon, R. D., A. S. Daloz, D. J. Vimont, and M. Biasutti, 2017a: Saharan Heat Low Biases in CMIP5 Models. *Journal of Climate*, **30** (8), 2867–2884.

Dixon, R. D., D. J. Vimont, and A. S. Daloz, 2017b: The relationship between tropical precipitation biases and the Saharan heat low bias in CMIP5 models. *Climate Dynamics*, 1–16.

747 Dong, B., and R. Sutton, 2015: Dominant role of greenhouse-gas forcing in the recovery of Sahel
748 rainfall. *Nature Climate Change*, **5**, 757–760.

749 d’Orgeval, T., J. Polcher, and L. Li, 2006: Uncertainties in modelling future hydrological change
750 over West Africa. *Climate dynamics*, **26** (1), 93–108.

751 Dunning, C. M., R. P. Allan, and E. Black, 2017: Identification of deficiencies in seasonal rainfall
752 simulated by CMIP5 climate models. *Environmental Research Letters*, **12** (11), 114 001.

753 Dunning, C. M., E. C. Black, and R. P. Allan, 2016: The onset and cessation of seasonal rainfall
754 over Africa. *Journal of Geophysical Research: Atmospheres*, **121** (19).

755 Dwyer, J. G., M. Biasutti, and A. H. Sobel, 2014: The effect of greenhouse gas–induced changes
756 in SST on the annual cycle of zonal mean tropical precipitation. *Journal of Climate*, **27** (12),
757 4544–4565.

758 Evan, A. T., C. Flamant, C. Lavaysse, C. Kocha, and A. Saci, 2015: Water vapor-forced green-
759 house warming over the Sahara Desert and the recent recovery from the Sahelian drought. *Jour-
760 nal of Climate*, **28** (1), 108–123.

761 Feng, X., A. Porporato, and I. Rodriguez-Iturbe, 2013: Changes in rainfall seasonality in the
762 tropics. *Nature Climate Change*, **3** (9), 811–815.

763 Frank, E., H. Eakin, and D. López-Carr, 2011: Social identity, perception and motivation in adap-
764 tation to climate risk in the coffee sector of Chiapas, Mexico. *Global environmental change*,
765 **21** (1), 66–76.

766 Funk, C., M. D. Dettinger, J. C. Michaelsen, J. P. Verdin, M. E. Brown, M. Barlow, and A. Hoell,
767 2008: Warming of the Indian Ocean threatens eastern and southern African food security but

could be mitigated by agricultural development. *Proceedings of the National Academy of Sciences*, **105** (32), 11 081–11 086.

Funk, C., and Coauthors, 2015: The climate hazards infrared precipitation with stations-a new environmental record for monitoring extremes. *Scientific data*, **2**.

Held, I. M., and B. J. Soden, 2006: Robust responses of the hydrological cycle to global warming. *Journal of Climate*, **19** (21), 5686–5699.

Howard, E., and R. Washington, 2018: Characterizing the Synoptic Expression of the Angola Low. *Journal of Climate*, **31** (17), 7147–7165, doi:10.1175/JCLI-D-18-0017.1.

Huffman, G. J., R. F. Adler, M. M. Morrissey, D. T. Bolvin, S. Curtis, R. Joyce, B. McGavock, and J. Susskind, 2001: Global precipitation at one-degree daily resolution from multisatellite observations. *Journal of Hydrometeorology*, **2** (1), 36–50.

Hulme, M., R. Doherty, T. Ngara, M. New, and D. Lister, 2001: African climate change: 1900–2100. *Climate research*, **17** (2), 145–168.

Hutchins, A., A. Tamargo, C. Bailey, and Y. Kim, 2015: Assessment of climate change impacts on cocoa production and approaches to adaptation and mitigation: a contextual view of Ghana and Costa Rica. *International Development Studies*, pg, **16**.

Issa Lélé, M., and P. J. Lamb, 2010: Variability of the Intertropical Front (ITF) and rainfall over the West African Sudan-Sahel zone. *Journal of Climate*, **23** (14), 3984–4004.

Joshi, M. M., J. M. Gregory, M. J. Webb, D. M. Sexton, and T. C. Johns, 2008: Mechanisms for the land/sea warming contrast exhibited by simulations of climate change. *Climate Dynamics*, **30** (5), 455–465.

Kniveton, D. R., R. Layberry, C. J. R. Williams, and M. Peck, 2009: Trends in the start of the wet season over Africa. *International Journal of Climatology*, **29** (9), 1216–1225.

Konare, A., A. Zakey, F. Solmon, F. Giorgi, S. Rauscher, S. Ibrah, and X. Bi, 2008: A regional climate modeling study of the effect of desert dust on the West African monsoon. *Journal of Geophysical Research: Atmospheres*, **113** (D12).

Lambert, F. H., M. J. Webb, and M. M. Joshi, 2011: The relationship between land–ocean surface temperature contrast and radiative forcing. *Journal of Climate*, **24** (13), 3239–3256.

Lavaysse, C., C. Flamant, S. Janicot, D. Parker, J.-P. Lafore, B. Sultan, and J. Pelon, 2009: Seasonal evolution of the West African heat low: a climatological perspective. *Climate Dynamics*, **33** (2-3), 313–330.

Lazenby, M. J., M. C. Todd, R. Chadwick, and Y. Wang, 2018: Future precipitation projections over central and southern africa and the adjacent indian ocean: What causes the changes and the uncertainty? *Journal of Climate*, **31** (12), 4807–4826, doi:10.1175/JCLI-D-17-0311.1.

Lazenby, M. J., M. C. Todd, and Y. Wang, 2016: Climate model simulation of the South Indian Ocean Convergence Zone: mean state and variability. *Climate Research*, **68** (1), 59–71.

Lee, J.-Y., and B. Wang, 2014: Future change of global monsoon in the CMIP5. *Climate Dynamics*, **42** (1-2), 101–119.

Liebmann, B., I. Bladé, G. N. Kiladis, L. M. Carvalho, G. B. Senay, D. Allured, S. Leroux, and C. Funk, 2012: Seasonality of African precipitation from 1996 to 2009. *Journal of Climate*, **25** (12), 4304–4322.

809 Liebmann, B., and Coauthors, 2017: Climatology and Interannual Variability of Boreal Spring
810 Wet Season Precipitation in the Eastern Horn of Africa and Implications for Its Recent Decline.
811 *Journal of Climate*, **30 (10)**, 3867–3886.

812 Maidment, R. I., R. P. Allan, and E. Black, 2015: Recent observed and simulated changes in
813 precipitation over Africa. *Geophysical Research Letters*, **42 (19)**, 8155–8164.

814 Maidment, R. I., D. Grimes, R. P. Allan, E. Tarnavsky, M. Stringer, T. Hewison, R. Roebeling,
815 and E. Black, 2014: The 30 year TAMSAT African Rainfall Climatology And Time series
816 (TARCAT) data set. *Journal of Geophysical Research: Atmospheres*, **119 (18)**, 10–619.

817 Maidment, R. I., and Coauthors, 2017: A new, long-term daily satellite-based rainfall dataset for
818 operational monitoring in Africa. *Scientific Data*, **4**.

819 Marteau, R., V. Moron, and N. Philippon, 2009: Spatial coherence of monsoon onset over Western
820 and Central Sahel (1950-2000). *Journal of Climate*, **22 (5)**, 1313–1324.

821 Marvel, K., M. Biasutti, C. Bonfils, K. E. Taylor, Y. Kushnir, and B. I. Cook, 2017: Observed and
822 Projected Changes to the Precipitation Annual Cycle. *Journal of Climate*, **30 (13)**, 4983–4995.

823 Monerie, P.-A., M. Biasutti, and P. Roucou, 2016: On the projected increase of Sahel rainfall
824 during the late rainy season. *International Journal of Climatology*, **36 (13)**, 4373–4383.

825 Monerie, P.-A., P. Roucou, and B. Fontaine, 2013: Mid-century effects of Climate Change on
826 African monsoon dynamics using the A1B emission scenario. *International Journal of Clima-*
827 *tology*, **33 (4)**, 881–896.

828 Monerie, P.-A., E. Sanchez-Gomez, and J. Boé, 2017: On the range of future Sahel precipitation
829 projections and the selection of a sub-sample of CMIP5 models for impact studies. *Climate*
830 *Dynamics*, **48 (7-8)**, 2751–2770.

831 Munday, C., and R. Washington, 2017: Circulation controls on southern African precipitation in
832 coupled models: The role of the Angola Low. *Journal of Geophysical Research: Atmospheres*,
833 **122 (2)**, 861–877.

834 Nicholson, S. E., 2000: The nature of rainfall variability over Africa on time scales of decades to
835 millenia. *Global and Planetary Change*, **26 (1)**, 137–158.

836 Nicholson, S. E., 2013: The West African Sahel: A review of recent studies on the rainfall regime
837 and its interannual variability. *ISRN Meteorology*, **2013**.

838 Nicholson, S. E., 2017: Climate and Climatic Variability of Rainfall over Eastern Africa. *Reviews*
839 *of Geophysics*.

840 Park, J.-y., J. Bader, and D. Matei, 2016: Anthropogenic Mediterranean warming essential driver
841 for present and future Sahel rainfall. *Nature Climate Change*, **6 (10)**, 941–945.

842 Parker, D., and M. Diop-Kane, 2017: Meteorology of Tropical West Africa: The Forecaster’s
843 Handbook. Wiley-Blackwell: Oxford, UK.

844 Pohl, B., C. Macron, and P.-A. Monerie, 2017: Fewer rainy days and more extreme rainfall by the
845 end of the century in Southern Africa. *Scientific Reports*, **7**.

846 Reason, C., W. Landman, and W. Tennant, 2006: Seasonal to decadal prediction of southern
847 African climate and its links with variability of the Atlantic Ocean. *Bulletin of the American*
848 *Meteorological Society*, **87 (7)**, 941–955.

849 Riahi, K., and Coauthors, 2011: RCP 8.5A scenario of comparatively high greenhouse gas emis-
850 sions. *Climatic Change*, **109 (1-2)**, 33.

851 Rosenthal, E., 2011: Heat damages Colombia coffee, raising prices. *The New York Times*, March,
852 **9**, 2011.

Rowell, D. P., C. A. Senior, M. Vellinga, and R. J. Graham, 2016: Can climate projection uncertainty be constrained over Africa using metrics of contemporary performance? *Climatic change*, **134** (4), 621–633.

Schmetz, J., P. Pili, S. Tjemkes, D. Just, J. Kerkmann, S. Rota, and A. Ratier, 2002: An introduction to Meteosat second generation (MSG). *Bulletin of the American Meteorological Society*, **83** (7), 977–992.

Seidel, D. J., Q. Fu, W. J. Randel, and T. J. Reichler, 2008: Widening of the tropical belt in a changing climate. *Nature Geoscience*, **1** (1), 21–24.

Seth, A., S. A. Rauscher, M. Biasutti, A. Giannini, S. J. Camargo, and M. Rojas, 2013: CMIP5 projected changes in the annual cycle of precipitation in monsoon regions. *Journal of Climate*, **26** (19), 7328–7351.

Shongwe, M., G. Van Oldenborgh, B. Van Den Hurk, B. De Boer, C. Coelho, and M. Van Aalst, 2009: Projected changes in mean and extreme precipitation in Africa under global warming. Part I: Southern Africa. *Journal of climate*, **22** (13), 3819–3837.

Shongwe, M. E., G. J. van Oldenborgh, B. van den Hurk, and M. van Aalst, 2011: Projected changes in mean and extreme precipitation in Africa under global warming. Part II: East Africa. *Journal of Climate*, **24** (14), 3718–3733.

Shonk, J. K., E. Guilyardi, T. Toniazzo, S. J. Woolnough, and T. Stockdale, 2018: Identifying causes of western pacific itcz drift in ecmwf system 4 hindcasts. *Climate Dynamics*, **50** (3-4), 939–954.

873 Sillmann, J., V. Kharin, F. Zwiers, X. Zhang, and D. Bronaugh, 2013: Climate extremes indices
874 in the CMIP5 multimodel ensemble: Part 2. Future climate projections. *Journal of Geophysical*
875 *Research: Atmospheres*, **118 (6)**, 2473–2493.

876 Solmon, F., M. Mallet, N. Elguindi, F. Giorgi, A. Zakey, and A. Konaré, 2008: Dust aerosol
877 impact on regional precipitation over western Africa, mechanisms and sensitivity to absorption
878 properties. *Geophysical Research Letters*, **35 (24)**.

879 Sultan, B., and S. Janicot, 2003: The West African monsoon dynamics. Part II: The "preonset"
880 and "onset" of the summer monsoon. *Journal of Climate*, **16 (21)**, 3407–3427.

881 Sutton, R. T., B. Dong, and J. M. Gregory, 2007: Land/sea warming ratio in response to climate
882 change: IPCC AR4 model results and comparison with observations. *Geophysical Research*
883 *Letters*, **34 (2)**.

884 Sylla, M. B., F. Giorgi, J. S. Pal, P. Gibba, I. Kebe, and M. Nikiema, 2015: Projected changes in
885 the annual cycle of high-intensity precipitation events over West Africa for the late twenty-first
886 century. *Journal of Climate*, **28 (16)**, 6475–6488.

887 Tanser, F. C., B. Sharp, and D. Le Sueur, 2003: Potential effect of climate change on malaria
888 transmission in Africa. *The Lancet*, **362 (9398)**, 1792–1798.

889 Tarnavsky, E., D. Grimes, R. Maidment, E. Black, R. P. Allan, M. Stringer, R. Chadwick, and
890 F. Kayitakire, 2014: Extension of the TAMSAT satellite-based rainfall monitoring over Africa
891 and from 1983 to present. *Journal of Applied Meteorology and Climatology*, **53 (12)**, 2805–
892 2822.

893 Taylor, C. M., and Coauthors, 2017: Frequency of extreme Sahelian storms tripled since 1982 in
894 satellite observations. *Nature*, **544 (7651)**, 475.

895 Taylor, K. E., R. J. Stouffer, and G. A. Meehl, 2012: An overview of CMIP5 and the experiment
896 design. *Bulletin of the American Meteorological Society*, **93** (4), 485–498.

897 Thomson, A. M., and Coauthors, 2011: RCP4. 5: a pathway for stabilization of radiative forcing
898 by 2100. *Climatic Change*, **109** (1-2), 77.

899 Tierney, J. E., C. C. Ummenhofer, and Coauthors, 2015: Past and future rainfall in the Horn of
900 Africa. *Science advances*, **1** (9), e1500682.

901 Van Vuuren, D. P., and Coauthors, 2011: The representative concentration pathways: an overview.
902 *Climatic change*, **109** (1-2), 5.

903 Vizzy, E. K., and K. H. Cook, 2017: Seasonality of the observed amplified Sahara warming trend
904 and implications for Sahel rainfall. *Journal of Climate*, **30** (9), 3073–3094.

905 Vizzy, E. K., K. H. Cook, J. Chimphamba, and B. McCusker, 2015: Projected changes in Malawis
906 growing season. *Climate Dynamics*, **45** (5-6), 1673–1698.

907 Yang, W., R. Seager, M. A. Cane, and B. Lyon, 2015a: The Annual Cycle of East African Precip-
908 itation. *Journal of Climate*, **28** (6), 2385–2404.

909 Yang, W., R. Seager, M. A. Cane, and B. Lyon, 2015b: The Rainfall Annual Cycle Bias over East
910 Africa in CMIP5 Coupled Climate Models. *Journal of Climate*, **28** (24), 9789–9802.

911 Zhang, L., P. Wu, T. Zhou, M. J. Roberts, and R. Schiemann, 2016: Added value of high resolution
912 models in simulating global precipitation characteristics. *Atmospheric Science Letters*, **17** (12),
913 646–657.

914 Zheng, X.-T., S.-P. Xie, Y. Du, L. Liu, G. Huang, and Q. Liu, 2013: Indian Ocean dipole response
915 to global warming in the CMIP5 multimodel ensemble. *Journal of Climate*, **26** (16), 6067–6080.

RCP 8.5 2080-2099 - Historical 1980-1999

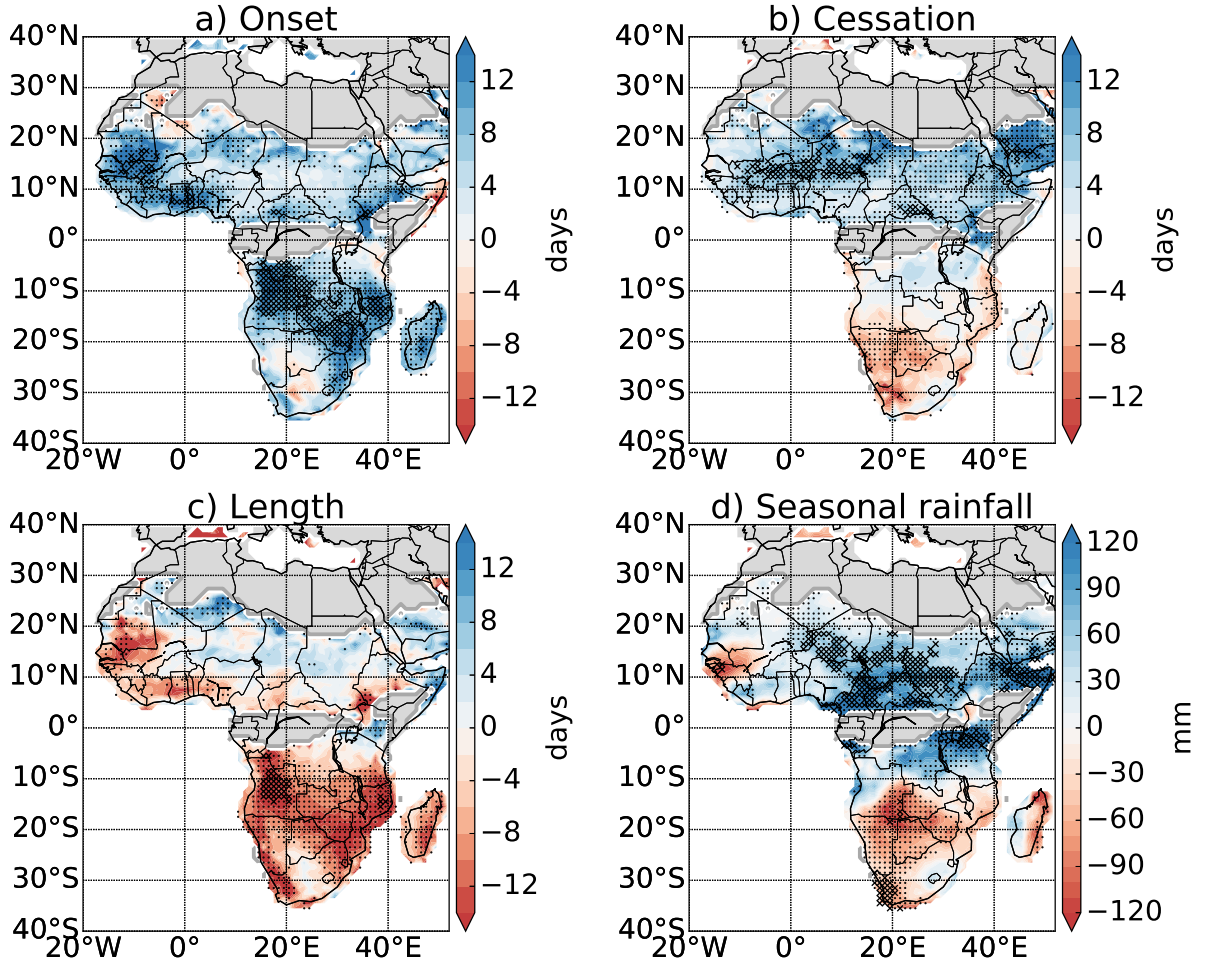


FIG. 1. Median Change in a) Onset, b) Cessation, c) Season Length and d) Wet Season Rainfall in 29 CMIP5 simulations from 1980-1999 (historical simulation) to 2080-2099 (RCP 8.5 scenario). Blue colours indicate the onset/cessation getting later while red colours indicate onset/cessation getting earlier. Crosses indicate where 75% of the simulations agree on the sign of the change, and more than 50% of the models show a statistically significant change (Mann Whitney U test, 5% significance level). Dots indicate where 75% of the simulations agree on the sign of the change. Grey regions indicate regions where <5 models produce onset/cessation dates due to a dry climate or two wet seasons per year.

RCP 8.5 2080-2099 - Historical 1980-1999

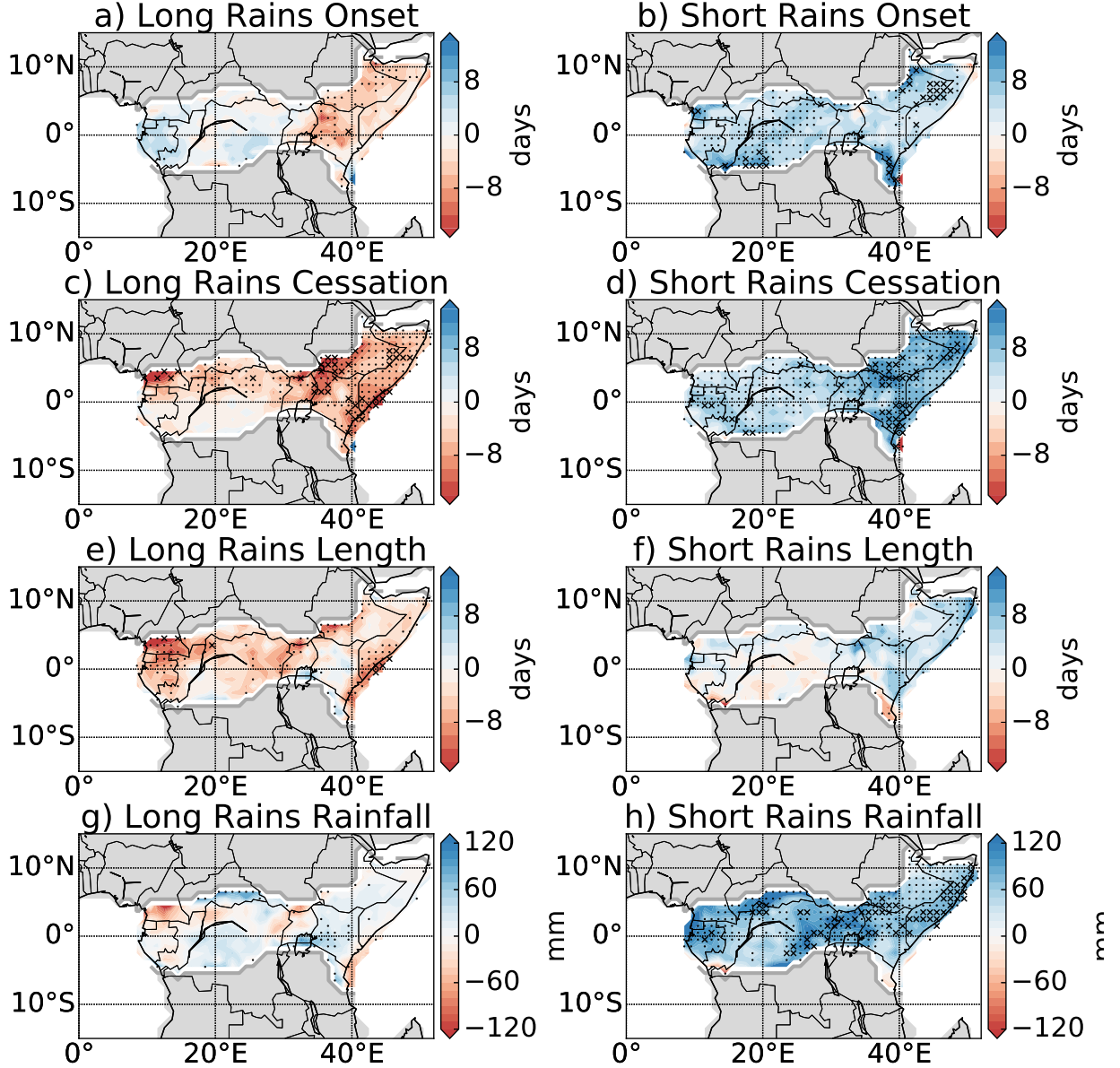


FIG. 2. Median Change in Onset (a-b), Cessation (c-d), Season Length (e-f) and Wet Season Rainfall (g-h) for the Long (boreal spring, left) and Short (boreal autumn, right) Rains in 29 CMIP5 simulations from 1980-1999 (historical simulation) to 2080-2099 (RCP 8.5 scenario). Blue colours indicate the onset/cessation getting later while red colours indicate onset/cessation getting earlier. Crosses indicate where 75% of the simulations agree on the sign of the change, and more than 50% of the models show a statistically significant change (Mann Whitney U test, 5% significance level). Dots indicate where 75% of the simulations agree on the sign of the change. Grey regions indicate regions where <5 models produce onset/cessation dates due to a dry climate or one wet season per year.

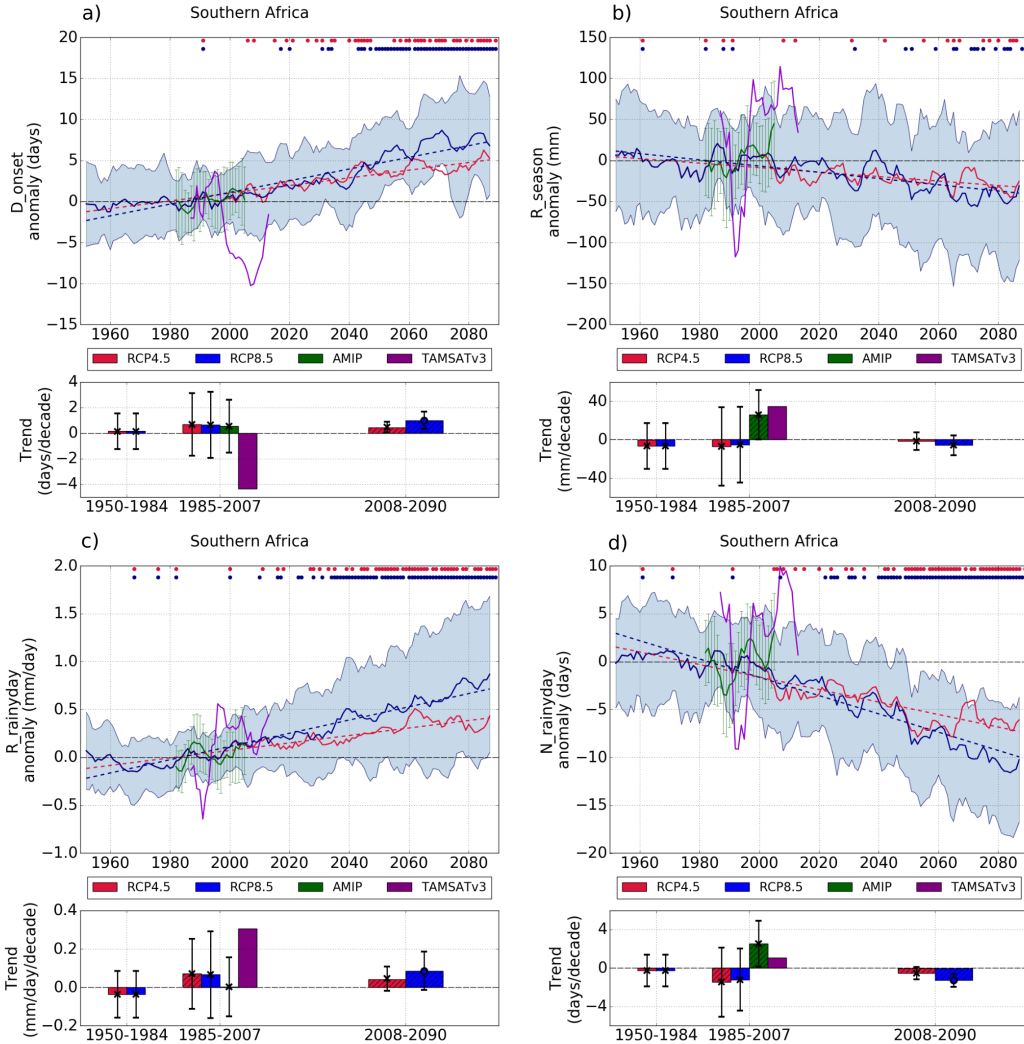


FIG. 3. Timeseries of a) Onset, b) Total Wet Season Rainfall, c) average rainfall per wet season rainy day ($\geq 1\text{mm}$) and d) number of rainy days ($\geq 1\text{mm}$) in the wet season over a region in Southern Africa (20°E - 35°E , 10°S - 20°S). The red and blue lines are the multi-model mean (over 29 CMIP5 models) after a 5 year running mean was applied, for RCP4.5 and RCP8.5 respectively over 1950-2090. The blue shaded area indicates the spread of model projections (\pm one standard deviation for RCP8.5 simulations - the spread for RCP4.5 was similar). The green line (with error bars) is the multi-model mean (\pm one standard deviation) for the AMIP simulations (1979-2008). The purple line is produced using TAMSATv3 precipitation (1985-2015). The dots indicate when the range of values from 29 models for that year are significantly different from the range for 1980-2000 at the 5% level, using a Mann Whitney U and t-test. The bar charts indicate the trend over different periods; 1950-1984, 1985-2007 (AMIP and observations period) and 2008-2090. The height of the bars indicates the trend of the multi-model mean; hatching indicates the trend is significantly different from 0 at the 5% level (Wald Test). The circle/cross and errorbar indicate the mean and standard deviations of the trend from the 29 models; a circle indicates over 50% of the models show a trend significantly different from 0 at the 5% level. Multi-model mean timeseries are computed after a 5 year moving average has been applied, and a 5 year moving average is also applied to the observation timeseries; trends are computed using the unsmoothed data.

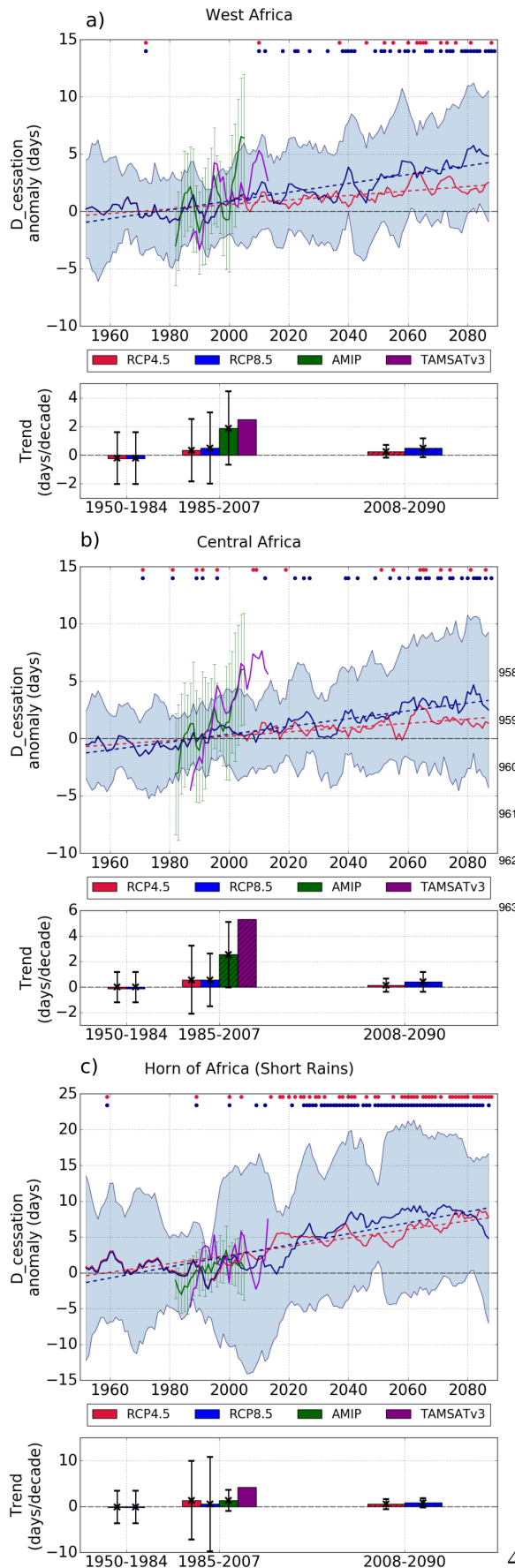


FIG. 4. As Figure 3 but for cessation over regions in a) West Africa (10°W - 9°E , 7°N - 13°N) and b) Central Africa (15°E - 30°E , 5°N - 11°N) which experience one wet season per year, and c) cessation of the short rains over the Horn of Africa (land points in 35°E - 51°E , 3°S - 12°N).

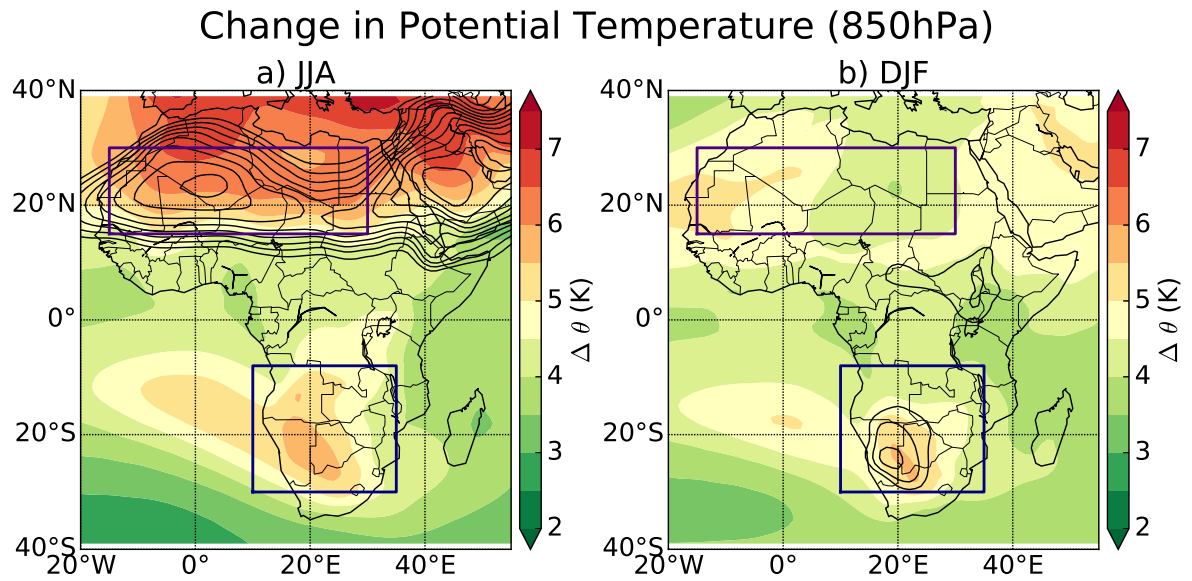


FIG. 5. Multi-model mean change in potential temperature (850hPa) for RCP 8.5 2080-2099 - historical 1980-1999 in a) JJA and b) DJF. Contours show the multi-model mean potential temperature (850hPa) in the historical simulation (1980-1999), increasing in steps of 1 K from 308 K. The purple and navy boxes indicate the regions used to compute the strength of the SHL and AL respectively.

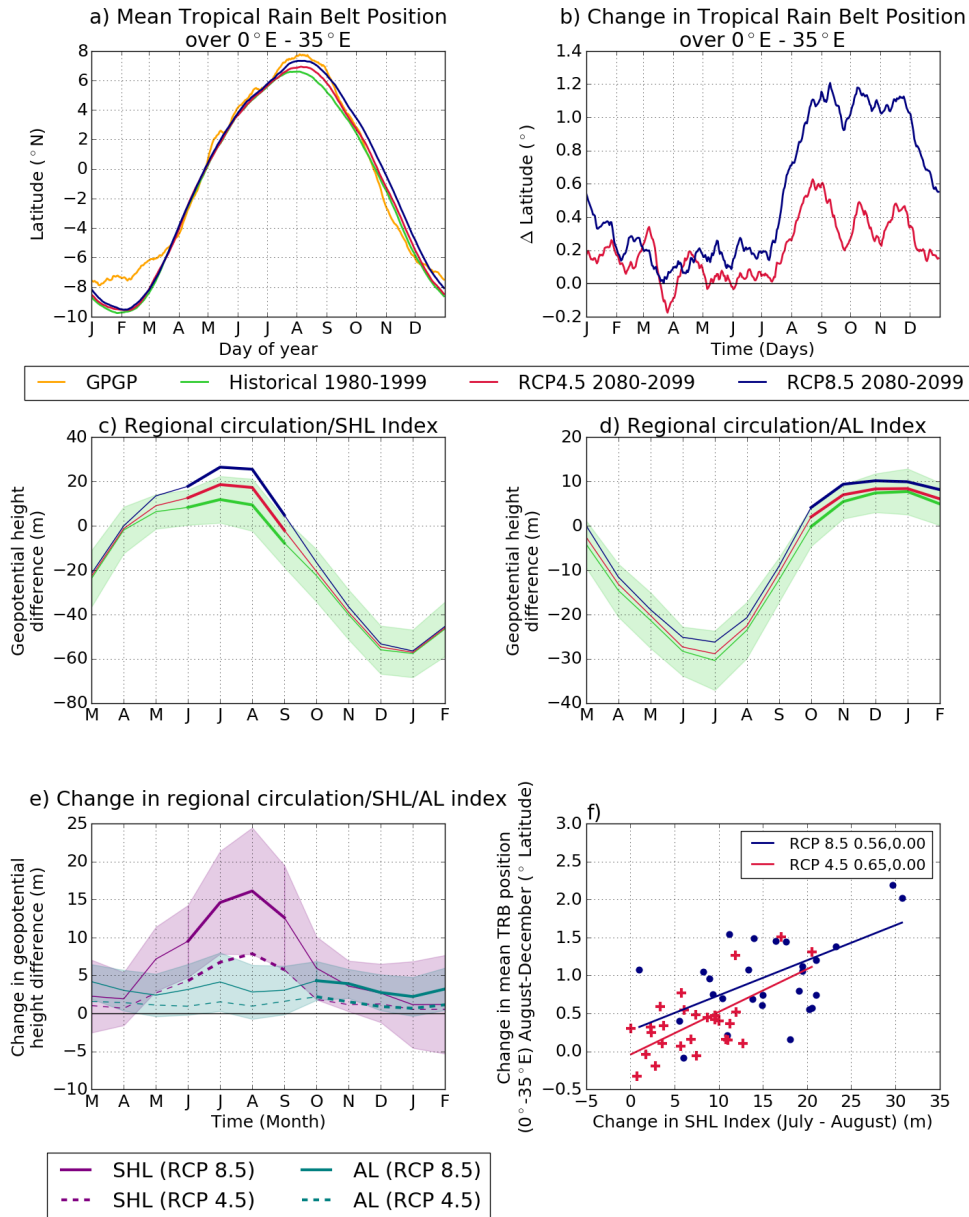


FIG. 6. Mean Tropical Rain Belt position (a) and change in position of the TRB (b) in RCP 4.5 and RCP 8.5 simulations over 29 CMIP5 models for 2080-2099 compared with historical 1980-1999 (and GPCP over 1997-2014 for a), averaged over 0°E-35°E, produced using the method of Shonk et al. (2018) on a daily basis and smoothed using a 15 day running mean. Regional circulation index for the northern region (including SHL, c) and southern region (including AL, d) for historical, RCP 4.5 and RCP 8.5 simulations over 29 CMIP5 models for 1980-1999 and 2080-2099. The green shaded area indicates the range across the 29 CMIP5 models for the historical simulation. The thicker lines indicate when the SHL/AL is within the region, and the regional circulation index also describes the strength of the SHL/AL. e) Change in strength of the regional circulation North/SHL (purple) and South/AL (teal) from historical 1980-1999 to RCP 4.5 (dashed) and RCP 8.5 (solid) (2080-2099). Again, thicker lines indicate when the SHL/AL is within the region, and the regional circulation index also describes the strength of the SHL/AL. The shading shows the model spread (\pm one standard deviation) for RCP 8.5. f) Mean change in position of TRB over 0°E-35°E (August-December) is plotted against change in SHL index for RCP 4.5 and RCP 8.5; the values in the legend indicate the Pearson correlation coefficient (r value, p value). EC-EARTH is excluded from (f).

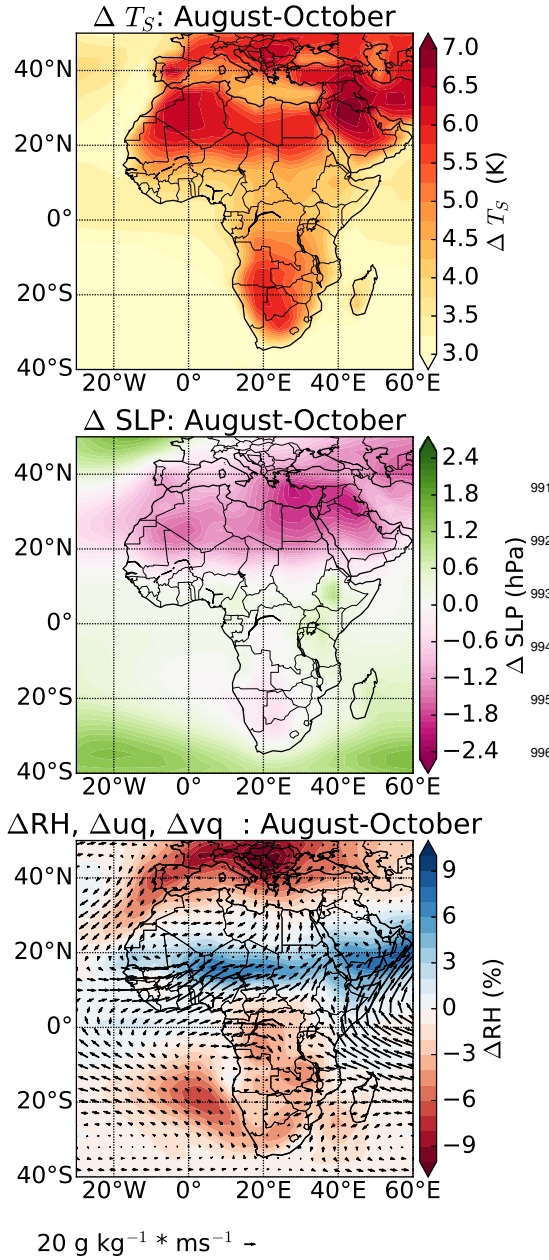


FIG. 7. Multi-model mean change in surface temperature (top, K), air pressure at sea level (middle, hPa) and relative humidity (%) and moisture flux ($\text{g kg}^{-1} \times \text{ms}^{-1}$) at 925hPa (bottom) from 1980-1999 (historical) to 2080-2099 (RCP8.5 simulation) over August-October.